

Article

Design of Smartphone-Assisted Point-of-Care Platform for Colorimetric Sensing of Uric Acid via Visible Light-Induced Oxidase-Like Activity of Covalent Organic Framework

Qi Kang, Yulong Xu and Xuwei Chen * 

College of Sciences, Northeastern University, Shenyang 110819, China

* Correspondence: chenxuwei@mail.neu.edu.cn

Abstract: Monitoring of uric acid (UA) levels in biological samples is of great significance for human health, while the development of a simple and effective method for the precise determination of UA content is still challenging. In the present study, a two-dimensional (2D) imine-linked crystalline pyridine-based covalent organic framework (TpBpy COF) was synthesized using 2,4,6-triformylphloroglucinol (Tp) and [2,2'-bipyridine]-5,5'-diamine (Bpy) as precursors via Schiff-base condensation reactions and was characterized with scanning electron microscopy (SEM), Energy dispersive X-ray spectroscopy (EDS), Powder X-ray diffraction (PXRD), Fourier transform infrared (FT-IR) spectroscopy, and Brunauer–Emmett–Teller (BET) assays. The as-synthesized TpBpy COF exhibited excellent visible light-induced oxidase-like activity, ascribed to the generation of superoxide radicals ($O_2^{\bullet-}$) by photo-generated electron transfer. TpBpy COF could efficiently oxidase the colorless substrate 3,3',5,5'-tetramethylbenzidine (TMB) into blue oxidized TMB (oxTMB) under visible light irradiation. Based on the color fade of the TpBpy COF + TMB system by UA, a colorimetric procedure was developed for UA determination with a detection limit of $1.7 \mu\text{mol L}^{-1}$. Moreover, a smartphone-based sensing platform was also constructed for instrument-free and on-site detection of UA with a sensitive detection limit of $3.1 \mu\text{mol L}^{-1}$. The developed sensing system was adopted for UA determination in human urine and serum samples with satisfactory recoveries (96.6–107.8%), suggesting the potential practical application of the TpBpy COF-based sensor for UA detection in biological samples.

Keywords: covalent organic framework; oxidase-like activity; colorimetric sensing; smartphone platform; uric acid



Citation: Kang, Q.; Xu, Y.; Chen, X. Design of Smartphone-Assisted Point-of-Care Platform for Colorimetric Sensing of Uric Acid via Visible Light-Induced Oxidase-Like Activity of Covalent Organic Framework. *Sensors* **2023**, *23*, 3881. <https://doi.org/10.3390/s23083881>

Academic Editors: Fengqing Yang and Liya Ge

Received: 21 February 2023

Revised: 30 March 2023

Accepted: 9 April 2023

Published: 11 April 2023



Copyright: © 2023 by the authors. Licensee MDPI, Basel, Switzerland. This article is an open access article distributed under the terms and conditions of the Creative Commons Attribution (CC BY) license (<https://creativecommons.org/licenses/by/4.0/>).

1. Introduction

Uric acid (UA) is the final oxidized product of purine metabolism in the human body [1]. Generally, UA usually exists in human urine and serum, and the normal concentration of UA is $1.4\text{--}4.5 \text{ mmol L}^{-1}$ in urine and $0.12\text{--}0.46 \text{ mmol L}^{-1}$ in serum [2]. The abnormal level of UA is usually a sign of some diseases, such as gout [3], renal disease [4], urolithiasis [5], and Lesh–Nyhan syndrome [6], and therefore the monitoring of UA contents in biological samples is of great significance to human health.

Up until now, various techniques have been developed for UA detection, including high-performance liquid chromatography (HPLC) [7], fluorescence spectroscopy [8], chemiluminescence [9], electrochemical techniques [10,11], etc. Typically, these detection processes usually adopt the dual natural enzyme reaction system based on uricase and horseradish peroxidase (HRP) [12], though most of these techniques are merited with high detection sensitivity, while intricate sample preparation and expensive instrumentations are usually needed to accomplish the detection (Table 1). Moreover, the poor stability and severe reaction condition of the catalysts adopted in these detection processes further restrict their practical applications. Recently, colorimetric detection technique based on

oxidase-mimic enzymes are gaining increasing attention due to the advantages of simplicity, rapidity, sensitivity, and low cost, and various materials, such as Q-graphene [13], metal-organic frameworks [14], noble metal nanoparticles [15], and alloy nanoparticles [16], have been used as artificial enzymes or enzymes mimetic for sensitive UA detection, attributed by their high efficiency of catalysis and kinetics similar to natural enzymes. Tarasankar et al. reported the colorimetric determination of UA with hierarchical porous Ni-MnO₂ nanoparticles based on the redox reaction between UA and oxTMB [17], which displayed a quite low detection limit. Wang et al. designed the MOF-based Pt nanoparticles (PtNPs@ZIF) with excellent peroxidase-like activity towards substrate TMB due to its unique electron transfer mechanism [18] and applied it to UA detection (as UA could suppress the oxidation of TMB). Liu et al. prepared core-shell silver-carbon dots (Ag-CDs) and nanocomposites with excellent peroxidase-like and surface-enhanced Raman scattering (SERS) activities [19], achieving the highly sensitive UA detection via the synergistic colorimetric reaction and enhanced SERS technique.

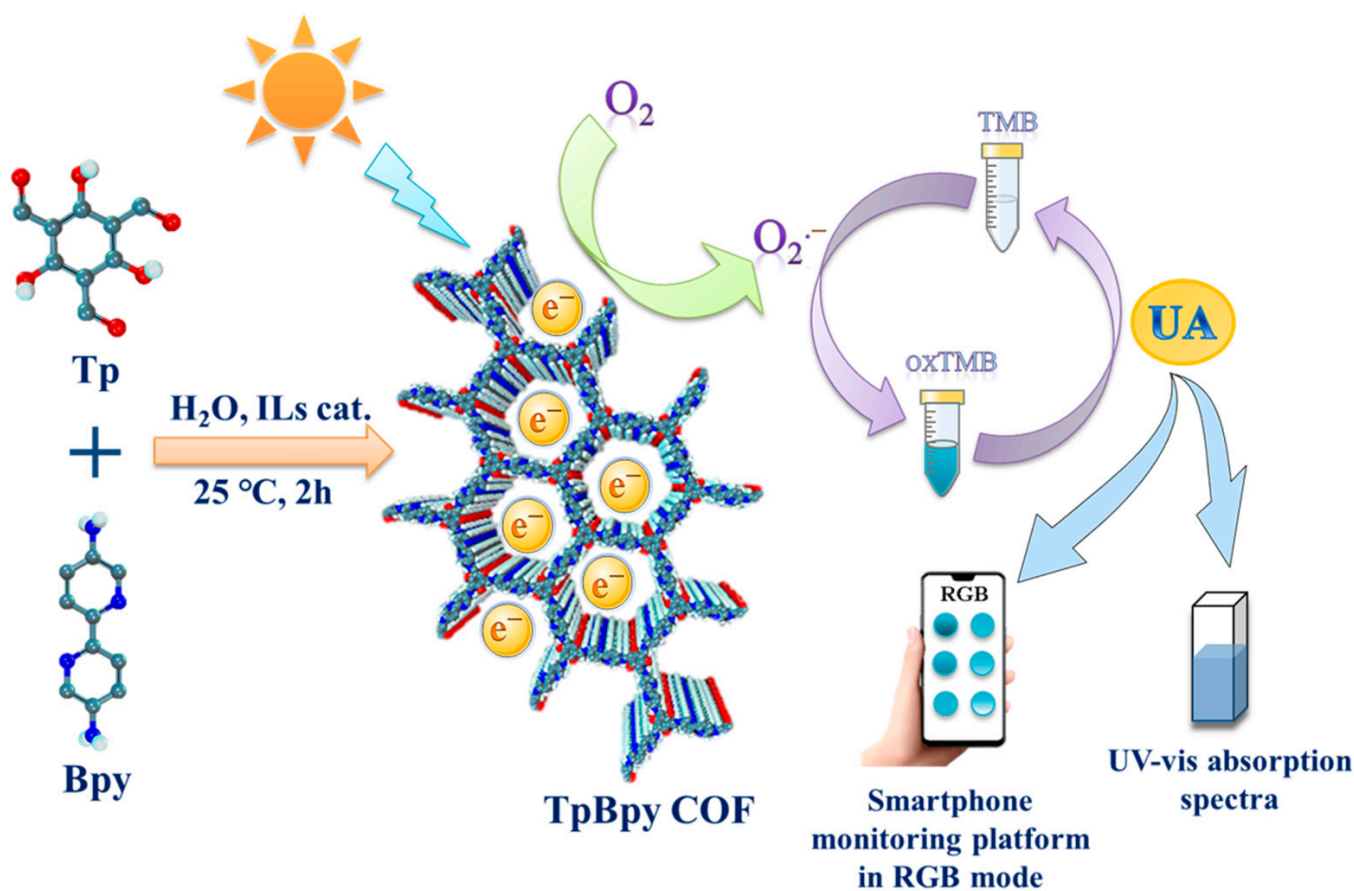
Table 1. Comparisons of different methods for UA detection.

Method	Sensitivity	Selectivity	Rapidity	Precision	Complex Sample Preparation Process	Expensive Instruments	Low Cost
Colorimetry	✓	✓	✓	x	x	x	✓
HPLC	✓	✓	✓	✓	✓	✓	x
Fluorescence	✓	✓	✓	✓	x	✓	✓
Chemiluminescence	✓	x	✓	✓	✓	x	✓
Electrochemistry	✓	✓	✓	✓	✓	x	✓

Covalent organic frameworks (COFs) as metal-free nanoenzymes have gained increasing attention for catalytic applications due to their excellent chemical stability, large surface area, high porosity, and tunable functionality that is superior to other porous materials. It is worth mentioning that some COF materials exhibit promising light-activated properties due to the fact that their C, N-rich skeleton structure endows them with the unique π - π array frameworks [20,21]. Lin et al. prepared two donor-acceptor heterosporous COFs (ETTA-Tz COF and ETTA-Td COF) by using 4,4'-(thiazolo [5,4-d]thiazole-2,5-diyl)dibenzaldehyde (Tz) or 4,4'-(benzo[c] [1,2,5]thiadiazole-4,7-diyl)dibenzaldehyde (Td) as precursors [22], and the narrow band gap and efficiently charge transport along the COF skeleton offered the as-prepared ETTA-Tz/ETTA-Td COF with excellent oxidase-like activity under light irradiation. Xu et al. reported a two-dimensional COF (TAS-COF) prepared by 2,4,6-triformylphloroglucinol (Tp) and 3,7-diaminodibenzo[b,d] thiophene sulfone (DAS), which owned excellent photocatalytic performance under visible light irradiation and was applied in the accurate determination of UO₂²⁺ content [23].

Recently, biosensors based on smartphone platforms have displayed great potential in the fields of healthcare monitoring [24–26], which is ascribed to the merits of portability, low cost, and easy operation. A smartphone can also be performed as an essential colorimetric detecting platform for field inspection, and the development of a smartphone-based platform for UA detection is worthy of consideration.

In the present study, a two-dimensional COF (TpBpy COF) with excellent photocatalytic performance was designed and synthesized via the Schiff-base condensation reaction of C₃-symmetric 2,4,6-triformylphloroglucinol (Tp) and C₂-symmetric [2,2'-bipyridine]-5,5'-diamine (Bpy) using ionic liquid as catalyst (Scheme 1). The as-synthesized TpBpy COF exhibited favorable oxidase-like activity under visible light irradiation, which could generate O₂^{•−} via photo-generated electron transfer. The generated O₂^{•−} could directly catalyze the oxidization of colorless TMB into blue oxidized TMB (oxTMB). The redox reaction between UA and oxidized TMB [27] induced obvious color fading of the TpBpy COF + TMB system, and thus a COF-based colorimetric sensor and a smartphone-based platform were developed for the sensitive sensing of UA content. The TpBpy COF-based colorimetric sensor and smartphone-based platform demonstrated their practicability by the accurate determination of UA contents in human serum and urine samples.



Scheme 1. The schematic diagram of UA detection based on the light-responsive TpBpy COF.

2. Materials and Methods

2.1. Chemicals and Reagents

2,4,6-triformylphloroglucinol (Tp) and [2,2'-bipyridine]-5,5'-diamine (Bpy) were purchased from Alpha Chemical Co., Ltd. (Zhengzhou, China). 3,3,5,5-tetramethyl-2,2'-bipyridine ethylbenzylidene (TMB), o-Phenylenediamine (OPD), and 2,2'-azino-bis(3-ethylbenzothiazoline-6-sulfonic acid) (ABTS) were provided by Aladdin Industrial Inc. (Shanghai, China). Uric acid (UA), HAc, and NaAc were obtained from Sinopharm Chemical Reagent (Shanghai, China). Ionic liquids [BmimN(CN)₂] were acquired from Chengjie Chemical Co., Ltd. (Shanghai, China).

Unless otherwise stated, all chemicals used were at least analytically pure and used without any purification. Notably, 18 MΩ cm deionized water was used in all experiments.

2.2. Synthesis of TpBpy COF

TpBpy COF was synthesized according to a reported procedure with some modifications [28]. Briefly, 0.08 mmol of Tp, 0.12 mmol of Bpy, and 100 μL of [BmimN(CN)₂] were dissolved in 2.0 mL H₂O, and, then, the mixture was stirred at room temperature for 2 h. Thereafter, the produced red solid was collected through centrifugation and was washed three times with acetone and ethanol, respectively. Finally, the product was dried under a vacuum at 60 °C for 12 h.

2.3. Characterization of TpBpy COF

Powder X-ray diffraction (PXRD) was collected on a Maxima XRD-7000 diffractometer (Shimadzu, Kyoto, Japan). N₂ adsorption-desorption isotherm was obtained by an Autosorb-IQ-MP-C automatic gas adsorption analyzer at 77 K (Quantachrome, Boynton Beach, FL, USA). Scanning electron microscopy (SEM) images were collected on a

SU8010 field-emission electron microscope at a voltage of 5.0 kV (Hitachi, Tokyo, Japan). Fourier transform infrared (FT-IR) spectra were recorded using a Nicolet-6700 FT-IR spectrophotometer (Thermo Scientific, Waltham, MA, USA). Ultraviolet-visible (UV-vis) absorption spectra were obtained on a U-3900 UV-Vis spectrophotometer (Hitachi, Tokyo, Japan). Visible light was generated by a white-light LED lamp ($\lambda \geq 420$ nm, power density = 62 mW cm^{-2} , Guanyu Lighting Co., Ltd., Guangzhou, China).

2.4. Steady-State Kinetic Studies of TpBpy COF as Oxidase-Mimic

The steady-state kinetic studies were carried out by changing the concentration of TMB under fixed TpBpy COF levels. In brief, 100 μL TMB of different concentrations and 50 μL COF solution (0.1 mg mL^{-1}) were mixed with 850 μL HAc-NaAc buffer (0.2 mol L^{-1} , pH 4.0). After irradiation with white-light LED lamp for 15 min, the absorbance at 652 nm was recorded.

2.5. Colorimetric Detection of UA

Typically, 50 μL COF solution (0.1 mg mL^{-1}) and 250 μL TMB solution (1.0 mmol L^{-1}) were mixed with 600 μL HAc-NaAc buffer (0.2 mol L^{-1} , pH 4.0), then 100 μL UA solution (prepared in 0.1 mol L^{-1} PBS buffer, pH 7.4) was added into the mixture subsequently, and the final volume of the detection system was 1 mL. After that, the resultant mixture was irradiated under a white-light LED lamp ($\lambda \geq 420$ nm, 62 mW cm^{-2}) for 15 min to stimulate the catalytic reaction. The absorbance of this system at 652 nm was recorded. The absorbance difference $A_0 - A$ (A_0 and A represent the absorbance at 652 nm in the absence/presence of UA) was adopted to fabricate the calibration curve.

2.6. Detection of UA by the Smartphone Mode

In an EP tube, 50 μL COF solution (0.1 mg mL^{-1}), 250 μL TMB solution (1.0 mmol L^{-1}), 100 μL UA solution (with different concentrations, $0.05\text{--}0.8 \text{ mmol L}^{-1}$), 600 μL HAc-NaAc buffer (0.2 mol L^{-1} , pH 4.0) were added and irradiated under a white-light LED lamp ($\lambda \geq 420$ nm, 62 mW cm^{-2}) for 15 min. Thereafter, removing 100 μL of the resultant mixture into a cover of centrifugal pipe. Digital images were collected in a self-made box ($19.5 \text{ cm} \times 18.5 \text{ cm} \times 16.5 \text{ cm}$) by a Mi 10 smartphone under a white-light LED lamp ($\lambda \geq 420$ nm, 62 mW cm^{-2}) through the "Color Grab" app and processed into R, G and B parameters. The distance between the smartphone's camera and the tested sample was 20 cm. The usage of LED lamp as the visible light source was due to its stable and intensive light irradiation.

2.7. Determination of UA Content in Real Samples

Human blood samples were provided by the Hospital of Northeastern with the volunteers' consent. The blood samples were dealt with refrigerating centrifugating (10,000 rpm) for 20 min, and then the collected supernatant was diluted 5-fold with 0.1 mol L^{-1} PBS buffer (pH 7.4).

Urine sample was donated by the author. The urine samples are 10-fold, diluted with 0.1 mol L^{-1} PBS buffer (pH 7.4), and then directed to colorimetric detection.

3. Results and Discussion

3.1. Synthesis and Characterizations of TpBpy COF

The TpBpy COF was synthesized via the Schiff-base condensation reaction between the electron-rich aromatic C_3 -symmetric Tp and C_2 -symmetric Bpy at room temperature, by using ionic liquids [BmimN(CN)₂] as a catalyst. The obtained TpBpy COF was an aggregate of nanorods and presented an irregular geometric shape (Figure 1A). The elemental composition of TpBpy COF was assessed by energy dispersive X-ray spectroscopy (EDS), and Figure 1B–D showed that the elements (C, N, O) of TpBpy COF were distributed evenly.

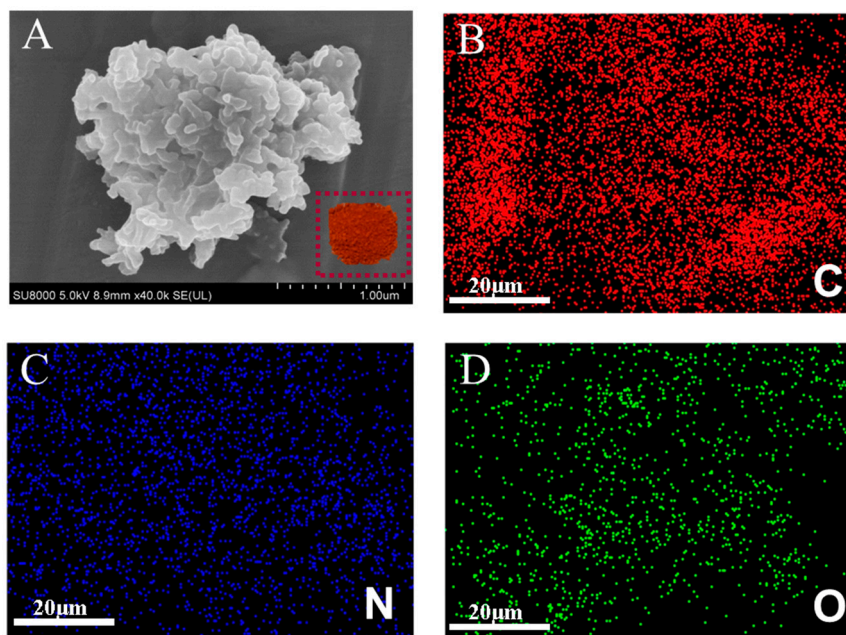


Figure 1. (A) SEM image of TpBpy COF (Insert: the picture of TpBpy COF). (B–D) EDS mapping of TpBpy COF.

Figure 2A showed the powder X-ray diffraction (PXRD) pattern of TpBpy COF. TpBpy COF showed an intense peak at $2\theta = 3.6^\circ$, and two weak peaks at $2\theta = 6.0^\circ$ and 26.0° , corresponding to the (100), (110), and (002) planes [29], which were in good agreement with the simulated PXRD pattern by the AA stacking mode. The intense peak at 3.6° suggested the presence of open channels in the as-synthesized COF, which is conducive to fast electron transfer [30].

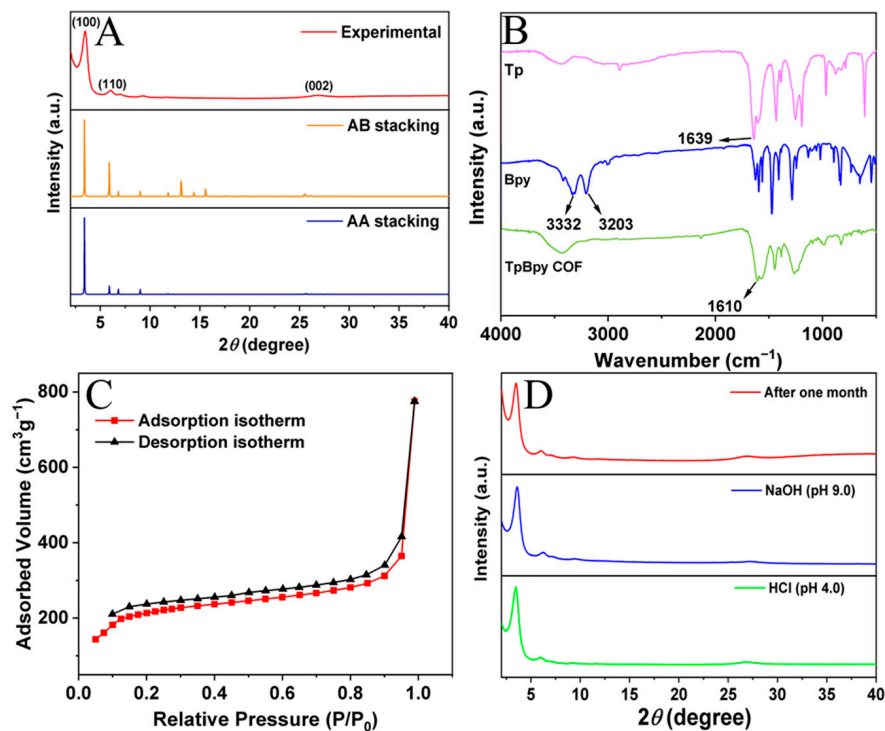


Figure 2. (A) Experimental and the simulated XRD pattern of TpBpy COF. (B) FT-IR spectra of Tp, Bpy, and TpBpy COF. (C) N₂ adsorption and desorption isotherm of TpBpy COF. (D) XRD pattern of TpBpy COF after one month of storage and treatment in HCl (pH 4.0) and NaOH (pH 9.0).

In the FT-IR spectra of Tp (Figure 2B), the presence of intense peak at $\sim 1639\text{ cm}^{-1}$ of Tp was attributed to the asymmetric stretching vibration of $-\text{C}=\text{O}$. For Bpy, the bands at $\sim 3203\text{ cm}^{-1}$ and $\sim 3332\text{ cm}^{-1}$ represented the stretching vibrations of $-\text{N}-\text{H}$ of aromatic amines. In the FT-IR of TpBpy COF, the $-\text{N}-\text{H}$ stretching bands (~ 3203 , $\sim 3332\text{ cm}^{-1}$) and the $-\text{C}=\text{O}$ stretching band ($\sim 1639\text{ cm}^{-1}$) disappeared due to the occurrence of Schiff-base condensation reactions, and a new characteristic peak appeared at $\sim 1610\text{ cm}^{-1}$, which can be attributed to the formed imine bond $-\text{C}=\text{N}$ [31].

The Brunauer–Emmett–Teller (BET) surface area of TpBpy COF was evaluated by N_2 adsorption and desorption measurement at 77 K (Figure 2C). The surface area of TpBpy COF was deduced to be $874.1\text{ m}^2\text{ g}^{-1}$, and the isotherm of TpBpy COF was accorded with type IV reversible adsorption isotherm [28,32], indicating the mesoporous structure of TpBpy COF. As shown in Figure 2D, the crystallinity of TpBpy COF was well maintained after one month of storage at room temperature. Compared with the pristine TpBpy COF, nearly no change was observed for the XRD pattern of the material after treatment with acid (pH 4.0 HCl) and base (pH 9.0 NaOH), indicating the excellent physical and chemical stability of the TpBpy COF.

3.2. Oxidase-Like Activity of TpBpy COF under Visible Light Illumination

The obtained TpBpy COF was mixed with three chromogenic substrates (TMB, ABTS, and OPD), and the resultant mixtures were irradiated with a white-light LED lamp ($\lambda \geq 420\text{ nm}$) for 15 min to explore the oxidase-like activity of TpBpy COF. The corresponding UV-vis absorption spectra were recorded.

As depicted in Figure 3A, compared with a single TMB, a distinct absorbance peak at 652 nm was found for the TMB + TpBpy COF system, and an obvious color change from colorless to blue was observed with the addition of TpBpy COF. Similarly, ABTS and OPD changed from colorless to green and yellow, respectively, with the presence of TpBpy COF, and the corresponding absorption peak appeared at 410 nm and 445 nm for ABTS + TpBpy COF and OPD + TpBpy COF system, attributing to the produce of oxABTS and oxOPD. Therefore, all the above results suggested that the TpBpy COF had excellent oxidase-like activity under visible light irradiation.

Figure 3B shows the HOMO and LUMO levels of TpBpy COF. DFT calculation results revealed that the LUMO position of TpBpy COF (-2.07 V vs. Ag/AgCl) was much more negative than that of $\text{O}_2/\text{O}_2^{\bullet-}$ redox potential (-0.33 V vs. Ag/AgCl) [33], suggesting that the electrons in the LUMO of TpBpy COF could theoretically reduce O_2 to generate $\text{O}_2^{\bullet-}$, which then oxidizes the colorless TMB into blue oxTMB. In order to verify that the oxidation of TMB was caused by the $\text{O}_2^{\bullet-}$ generated by TpBpy COF, the electron paramagnetic resonance (EPR) analysis was carried out to figure out the generation of $\text{O}_2^{\bullet-}$ by using 5,5-dimethyl-1-pyrroline N-oxide (DMPO) as radical trappers. As shown in Figure 3C, the signal of $\text{O}_2^{\bullet-}$ was clearly observed after light irradiation for 20 min, confirming that the generation of $\text{O}_2^{\bullet-}$ was caused by photo-induced electron transfer of TpBpy COF.

To understand the kinetic mechanism of the oxidase-like activity of TpBpy COF, apparent steady-state kinetic parameters of the catalytic oxidation reaction are determined by changing the concentrations of TMB under fixed TpBpy COF levels. A series of initial reaction rates are calculated and applied to the double reciprocal of the Michaelis–Menten equation [29]:

$$V = V_{max} [S]/(K_m + [S])$$

where $[S]$ was TMB content, K_m resembles the Michaelis–Menten constant, V was the initial velocity of the reaction, and V_{max} was the maximal velocity of TMB oxidation.

As shown in Figure 3D, the absorbance increased gradually with TMB concentration. The results obtained from Lineweaver–Burk plots indicated that the Michaelis–Menten constant (K_m) and the maximum initial velocity (V_{max}) of TpBpy COF were deduced to be $94.8\text{ }\mu\text{mol L}^{-1}$ and $4.31 \times 10^{-6}\text{ M min}^{-1}$, respectively. Generally, K_m has been identified as an indicator of enzyme affinity with substrates. Compared with other oxidase-like catalysts

(Table 2), the K_m value of TpBpy COF was lower, suggesting the stronger affinity of TpBpy COF toward TMB than other oxidase-like catalysts.

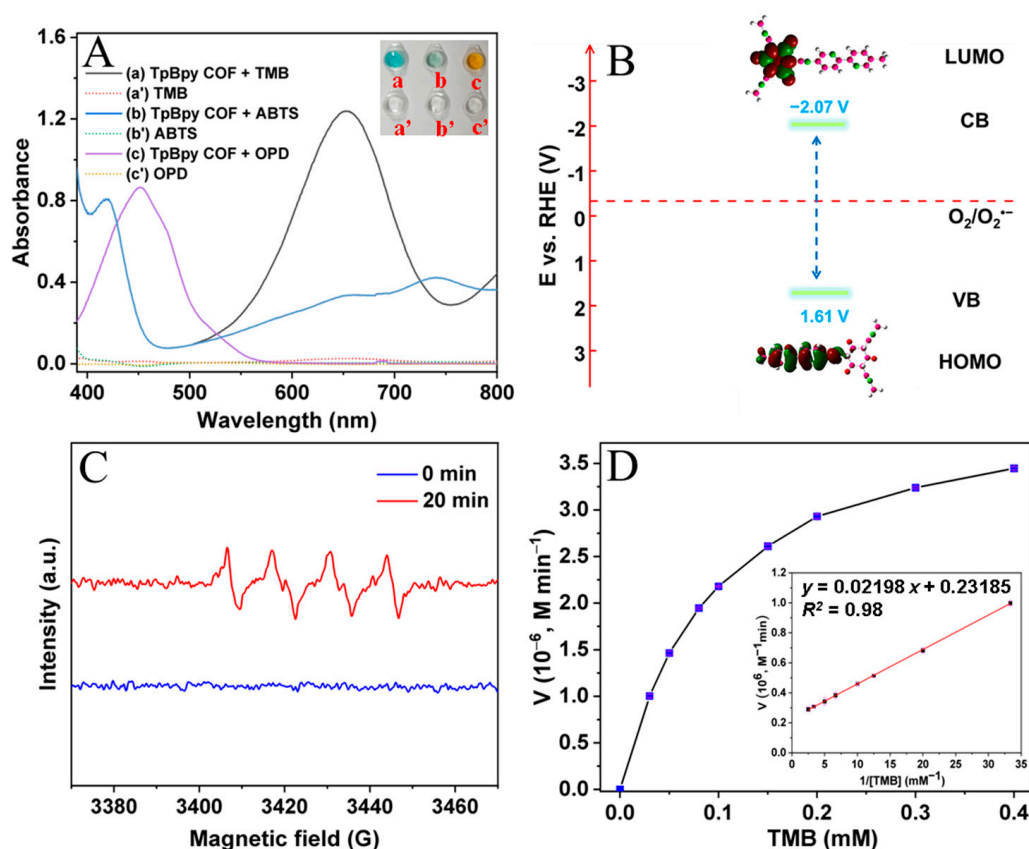


Figure 3. (A) UV-vis spectra of different chromogenic substrates with/without TpBpy COF in the HAC-NaAc buffer (0.2 mol L^{-1} , pH 4.0). Insert: the images of the system containing TMB (a, a'), APTS (b, b'), and OPD (c, c'). (B) Density functional theory (DFT) calculation of TpBpy COF (Insert: the images of LUMO and HOMO). (C) EPR spectra of TpBpy COF after illumination under white-light LED lamp for 20 min and under dark environment. (D) Michaelis–Menten and Lineweaver–Burk curves of TpBpy COF against the different concentrations of TMB.

Table 2. The kinetic parameters of oxidation reactions catalyzed by reported enzyme-like nanomaterials and horseradish peroxidase.

Catalyst	K_m (mM)	V_m ($10^{-6} \text{ M min}^{-1}$)	Ref.
TpBpy COF	0.0948	4.31×10^{-6}	This work
PtNPs@ZIF	0.15	7.26×10^{-6}	[18]
CuSNPs	0.216	1.45×10^{-5}	[34]
Fe_3O_4 @MIL-100 (Fe)	0.112	6.85×10^{-6}	[35]
HRP	0.4340	6.00×10^{-6}	[23]

3.3. Analytical Performance for Colorimetric UA Sensing

The above investigations revealed that the TpBpy COF exhibited favorable oxidase-like activity and could oxidize the colorless TMB into blue oxTMB. Meanwhile, it has been demonstrated that UA was able to reduce the blue oxTMB into colorless TMB [21,27]. Figure 4A showed the recorded UV-vis spectra of the TpBpy COF + TMB system before/after the addition of UA. It could be seen that the presence of UA induced an obvious decrease in the absorbance of the TpBpy COF + TMB system, and thus a colorimetric procedure was developed for UA sensing.

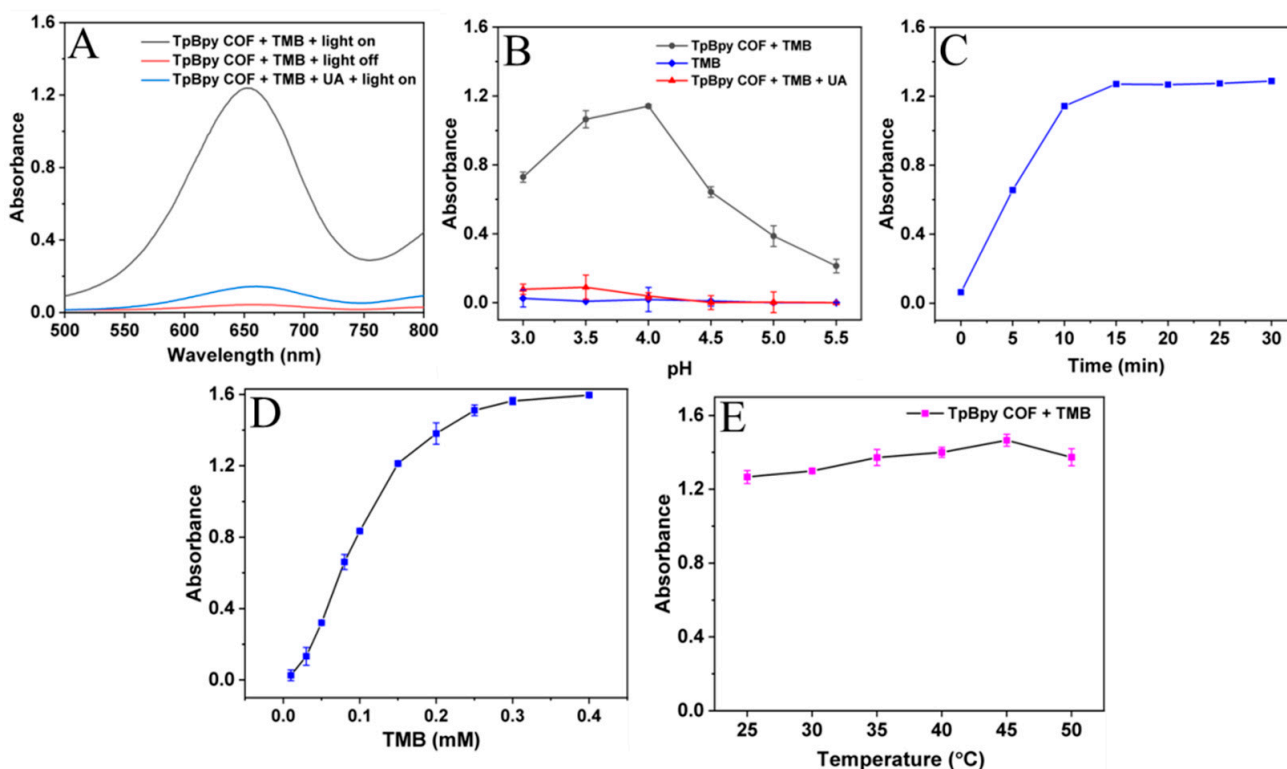


Figure 4. (A) UV-vis spectra of TpBpy COF + TMB system with/without the presence of UA. (B) The effect of pH on the absorbance at 652 nm of TpBpy COF + TMB, TpBpy COF, TMB, TpBpy COF + TMB + UA under visible light irradiation. The effect of irradiation time (C), TMB concentration (D), and temperature (E) on the absorbance at 652 nm of TpBpy COF + TMB.

To achieve the best UA sensing performance, experimental parameters, including pH value, irradiation time, and TMB concentration, were optimized. It was found that TpBpy COF presented the highest oxidase-like activity under pH 4.0 (Figure 4B), and the absorbance difference of TMB + TpBpy COF system with/without UA reached the maximum at the same pH condition. The reason might be connected to the fact that TMB oxidation tends to form yellow diimine in excessive acid conditions and the decreased solubility of TMB under high pH conditions. Figure 4C illustrated the influence of irradiation time. The absorbance signal firstly increased obviously with the irradiation time, and, then, kept relatively stable when the irradiation time was longer than 15 min. The effect of TMB concentration was investigated in the range of 0.01–0.4 mmol L⁻¹ (Figure 4D). The absorbance difference increased rapidly with the TMB content up to 0.25 mmol L⁻¹, and then the signal increase became slow with the further increase in TMB concentrations. Figure 4E shows the influence of temperature. It is obvious that the increase in temperature just contributed slightly to the oxidase-like activity of TpBpy COF. For the comprehensive consideration of manipulation convenience and detection sensitivity, UA detection was carried out under a temperature of 25 °C in the present study.

Based on the comprehensive consideration of detection sensitivity and analytical cost, the colorimetric sensing procedure for UA detection was performed under pH 4.0, with an irradiation time of 15 min and a TMB concentration of 0.25 mmol L⁻¹.

Figure 5A illustrates the spectra of the TpBpy COF + TMB system with the addition of different concentrations of UA under optimal conditions. The absorbance difference ($A_0 - A$) presented a good linear relationship with UA in the concentration range of 5–80 $\mu\text{mol L}^{-1}$ ($R^2 = 0.98$) (Figure 5B), and the limit of detection (LOD, $3\sigma/k$) was deduced to be 1.7 $\mu\text{mol L}^{-1}$. Table 3 summarized the performance of reported materials for UA sensing. It could be seen that TpBpy COF-based sensing system provided improved sensing sensitivity due to the excellent oxidase-like activity of TpBpy COF.

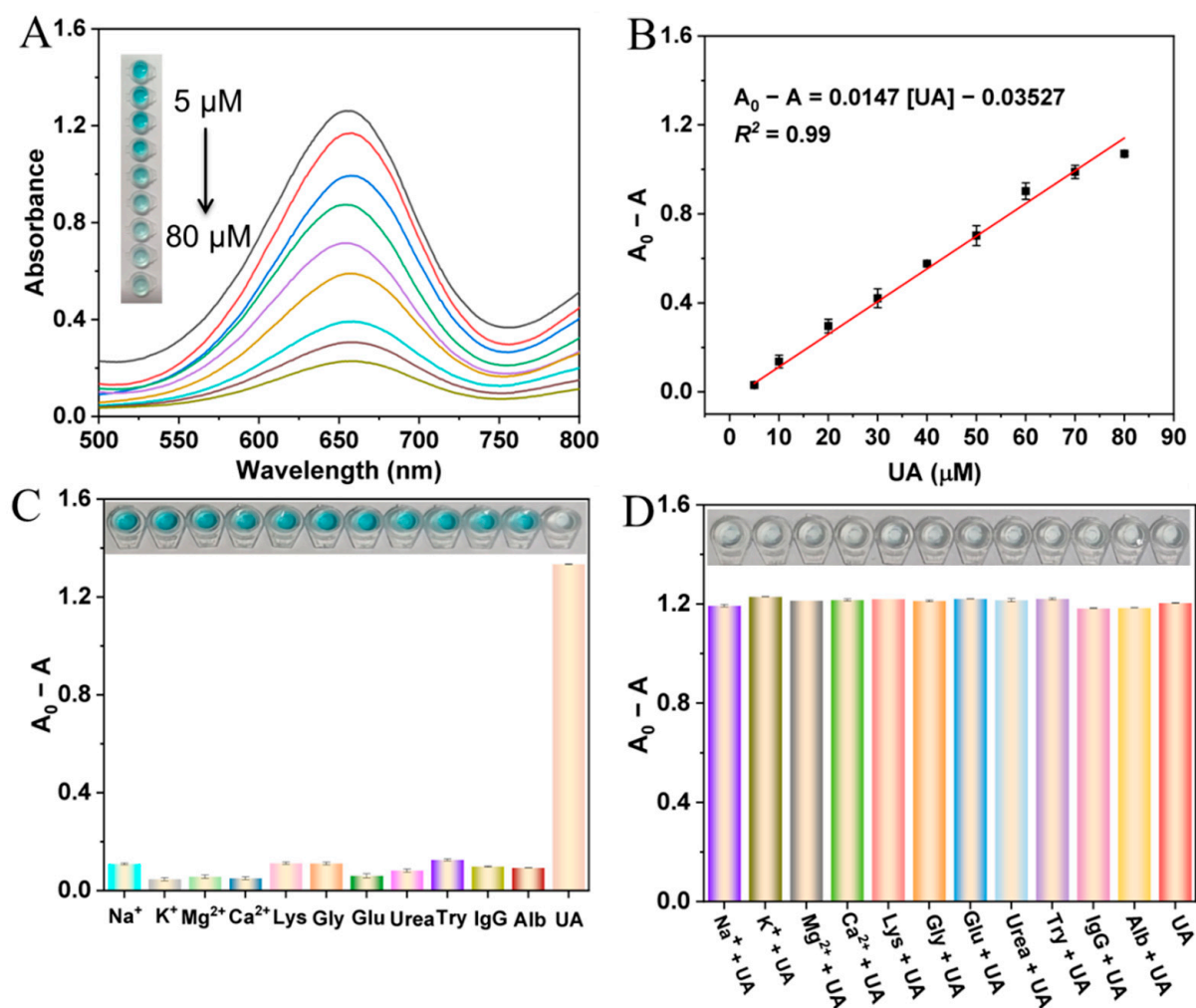


Figure 5. (A) UV-vis spectra of the TpBpy COF + TMB system toward different concentrations of UA (from up to down: 5, 10, 20, 30, 40, 50, 60, 70, and 80 μmol L⁻¹). Inset: the images of the corresponding solutions. (B) The linear relationship between the absorbance difference ($A_0 - A$) and UA content (A_0 and A represented the absorbance at 652 nm in the absence/presence of UA). (C) The response of TpBpy COF + TMB system towards UA and various interferences. (D) The signal response of TpBpy COF + TMB system towards UA coexisting with other substrates. The concentration of UA was 100 μmol L⁻¹, IgG and Alb was 1 mg L⁻¹ and the concentration of other interferences was 1 mmol L⁻¹.

Table 3. The analytical performance of reported materials for UA sensing.

Material	Linear Range (μM)	LOD (μM)	Ref.
TpBpy COF	5–80	1.7	This work
Uricase/graphitic carbon nitride	10–100	8.9	[36]
Ni glancing angle deposition film	0–6	3.3	[37]
Lanthanide-doped upconversion nanoparticles	10–1000	2.86	[38]
Au/Ag nanoclusters	5–50	5.1	[39]
TCPO-H ₂ O ₂ -rubrene	10–1000	5	[40]
Photochemically reduced graphene oxide	40–415	8	[41]

To evaluate the selectivity of the TpBpy COF-based system for UA sensing, the response of the sensing system was investigated in the presence of potentially interfering substances that coexisted in biological samples, including Na^+ , K^+ , Mg^{2+} , Ca^{2+} , lysine (Lys), glycine (Gly), tryptophan (Try), glucose (Glu), urea, albumin (Alb), and immunoglobulin (IgG). As illustrated in Figure 5C, only the UA induced obvious color fading and significant absorbance reduction in comparison with other substances. Moreover, those potential interfering substances nearly pose no influence on the signal of the sensing system when they coexisted with UA (Figure 5D). These demonstrated the favorable anti-interference ability of the TpBpy COF-based sensing system.

3.4. Smartphone Sensing Platform for UA Detection

Due to the fact that the presence of UA could induce obvious color fading of the TpBpy COF-based sensing system, a smartphone-based platform was further developed for instrument-free and on-site detection of UA. The high-resolution photos of the sensing system with different UA concentrations under white-light irradiation were captured and converted into color intensity based on RGB mode by the “Color Grab” app. The YUV color space method with a weighted average of R, G, and B components recommended by the International Telecommunication Union (ITU) was adopted to construct luminance and color-difference signals [42], and the color intensity was calculated by using the following formula: $I = 0.3 R + 0.59 G + 0.11 B$ [43]. As shown in Figure 6, the calculated RGB value “I” exhibited a good linear relationship in the UA concentration range of 5–80 $\mu\text{mol L}^{-1}$ ($R^2 = 0.99$), giving access to the UA detection by a portable smartphone independent of lab equipment, and the detection limit was 3.1 $\mu\text{mol L}^{-1}$.

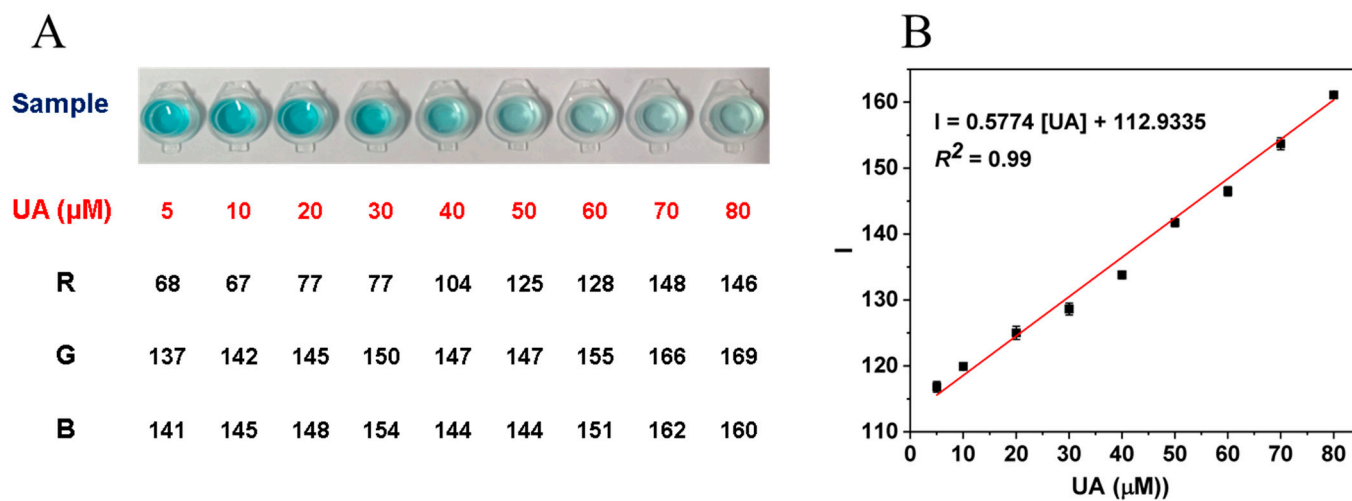


Figure 6. (A) Color changes in the TpBpy COF + TMB system and the corresponding RGB value with various content of UA (Red words represent different concentrations of UA). (B) The linear response of color intensity acquired by the RGB mode under different UA concentrations.

3.5. Determination of UA Content in Human Serum and Urine Samples

To verify the practicability of this TpBpy COF-based sensing system, UA content in human urine and serum samples were determined via the colorimetric procedure and the smartphone-based platform.

As shown in Table 4, the spiked recoveries for UA in urine samples and serum samples were 97.2–107.8% and 96.6–100.2%, respectively. Meanwhile, the UA contents in the biological samples that determined the TpBpy COF-based colorimetric procedure were in good agreement with that obtained by means of a smartphone-based platform. All these results revealed that the TpBpy COF-based sensor owns great potential in the detection of UA contents in practical applications.

Table 4. Determination of UA content in human urine and serum samples ($n = 3$).

Sample	Added (μM)	Colorimetric Determination (μM)	Recovery (%)	RSD (% , $n = 3$)	Smartphone Determination (μM)	Recovery (%)	RSD (% , $n = 3$)
Urine	0	24.3 ± 1.2		4.8	23.3 ± 0.8		3.3
	10.0	34.7 ± 2.0	103.6 ± 2.0	5.6	34.1 ± 0.6	107.1 ± 5.6	1.6
	30.0	55.0 ± 1.1	102.3 ± 3.5	1.9	55.7 ± 0.6	107.8 ± 2.0	1.1
	50.0	73.0 ± 0.7	97.2 ± 1.3	0.9	73.8 ± 1.6	100.8 ± 3.2	2.3
Serum	0	4.5 ± 0.2		3.6	4.6 ± 0.1		2.4
	10.0	14.3 ± 0.4	98.8 ± 3.5	2.7	14.3 ± 0.9	97.1 ± 0.8	5.9
	30.0	33.9 ± 0.4	98.1 ± 1.4	1.3	33.6 ± 0.4	96.6 ± 1.4	1.2
	50.0	54.5 ± 0.4	100.1 ± 0.9	0.7	54.7 ± 0.8	100.2 ± 1.6	1.4

4. Conclusions

In this study, we successfully synthesized a two-dimensional covalent organic framework TpBpy COF via the Schiff-base condensation reaction. The as-synthesized TpBpy COF exhibited excellent oxidase-like activity under visible light irradiation that could efficiently catalyze the TMB into blue oxTMB. Based on the ability of UA to reduce oxTMB, we proposed two modes (batch colorimetric procedure and smartphone signal readout platform) for UA sensing. The UA contents determined by the smartphone-based signal readout platform are consistent with the theoretic UA contents in healthy human serum and urine [2], suggesting that the TpBpy COF-based smartphone signal readout system is able to act as a powerful platform for point-of-care UA content evaluation free of sophisticated instruments, which might provide useful and timely information for preliminary screening of UA-related diseases.

Author Contributions: Conceptualization, Q.K. and Y.X.; methodology, Q.K.; software, Q.K.; validation, Q.K. and Y.X.; investigation, Q.K.; data curation, Q.K.; writing—original draft preparation, Q.K.; writing—review and editing, Y.X. and X.C.; supervision, X.C.; project administration, X.C.; funding acquisition, X.C. All authors have read and agreed to the published version of the manuscript.

Funding: This research was funded by the Liao Ning Science and Technology Development Foundation Guided by Central Government (2022JH6/100100024).

Institutional Review Board Statement: Not applicable.

Informed Consent Statement: Not applicable.

Data Availability Statement: The data presented in this work are available in the article.

Conflicts of Interest: The authors declare no conflict of interest.

References

- Huang, S.; Shi, Y.; Wu, C.; Yuan, C.; Yang, Y.; Li, Y.; Wu, T. Detection of serum uric acid using the optical polymeric enzyme biochip system. *Biosens. Bioelectron.* **2004**, *19*, 1627–1633. [[CrossRef](#)] [[PubMed](#)]
- Badoei-Dalfard, A.; Sohrabi, N.; Karami, Z.; Sargazi, G. Fabrication of an efficient and sensitive colorimetric biosensor based on Uricase/Th-MOF for uric acid sensing in biological samples. *Biosens. Bioelectron.* **2019**, *141*, 111420. [[CrossRef](#)]
- Zhang, L.; Zhang, C.; Zhuang, Z.; Li, C.; Pan, P.; Zhang, C.; Zhang, X. Bio-inspired nanoenzyme for metabolic reprogramming and anti-inflammatory treatment of hyperuricemia and gout. *Sci. China Chem.* **2021**, *64*, 616–628. [[CrossRef](#)]
- Nakagawa, T.; Kang, D.; Feig, D.; Sanchez-Lozada, L.; Srinivas, T.; Sautin, Y.; Ejaz, A.; Segal, M.; Johnson, R. Unearthing uric acid: An ancient factor with recently found significance in renal and cardiovascular disease. *Kidney Int.* **2006**, *69*, 1722–1725. [[CrossRef](#)] [[PubMed](#)]
- Srinivasan, S.; Kalaiselvi, P.; Sakthivel, R.; Pragasa, V.; Muthu, V.; Varalakshmi, P. Uric acid: An abettor or protector in calcium oxalate urolithiasis? Biochemical study in stone formers. *Clin. Chim. Acta* **2005**, *353*, 45–51. [[CrossRef](#)]
- Maramattom, B.V. Self-mutilation in the Lesch-Nyhan syndrome. *Neurology* **2005**, *65*, E25. [[CrossRef](#)] [[PubMed](#)]
- Remane, D.; Grunwald, S.; Hoeke, H.; Mueller, A.; Roeder, S.; von Bergen, M.; Wissenbach, D. Validation of a multi-analyte HPLC-DAD method for determination of uric acid, creatinine, homovanillic acid, niacinamide, hippuric acid, indole-3-acetic acid and 2-methylhippuric acid in human urine. *J. Chromatogr. B* **2015**, *998*, 40–44. [[CrossRef](#)]
- Kong, R.; Yang, A.; Wang, Q.; Wang, Y.; Ma, L.; Qu, F. Uricase based fluorometric determination of uric acid based on the use of graphene quantum dot@silver core-shell nanocomposites. *Microchim. Acta* **2018**, *185*, 63. [[CrossRef](#)]

9. Saqib, M.; Qi, L.; Hui, P.; Nsabimana, A.; Halawa, M.; Zhang, W.; Xu, G. Development of luminol-N-hydroxyphthalimide chemiluminescence system for highly selective and sensitive detection of superoxide dismutase, uric acid and Co^{2+} . *Biosens. Bioelectron.* **2018**, *99*, 519–524. [[CrossRef](#)]
10. Kumar, A.; Shanmugam, R. Simple method for simultaneous detection of uric acid, xanthine and hypoxanthine in fish samples using a glassy carbon electrode modified with as commercially received multiwalled carbon nanotubes. *Anal. Methods* **2011**, *3*, 2088–2094. [[CrossRef](#)]
11. Liao, L.; Liao, C.; Liu, C.; Yang, T.; Wang, G. Evaluation of an electrochemical biosensor for uric acid measurement in human whole blood samples. *Clin. Chim. Acta* **2014**, *436*, 72–77. [[CrossRef](#)]
12. Lu, H.; Li, J.; Zhang, M.; Wu, D.; Zhang, Q. A highly selective and sensitive colorimetric uric acid biosensor based on Cu(II)-catalyzed oxidation of 3,3',5,5'-tetramethylbenzidine. *Sens. Actuators B Chem.* **2017**, *244*, 77–83. [[CrossRef](#)]
13. Li, S.; Zhao, X.; Gang, R.; Cao, B.; Wang, H. Doping nitrogen into Q-graphene by plasma treatment toward peroxidase mimics with enhanced catalysis. *Anal. Chem.* **2020**, *92*, 5152–5157. [[CrossRef](#)]
14. Liu, Z.; Wang, F.; Ren, J.; Qu, X. A series of MOF/Ce-based nanozymes with dual enzyme-like activity disrupting biofilms and hindering recolonization of bacteria. *Biomaterials* **2019**, *208*, 21–31. [[CrossRef](#)]
15. Deng, H.; Lin, X.; Liu, Y.; Li, K.; Zhuang, Q.; Peng, H.; Liu, A.; Xia, X.; Chen, W. Chitosan-stabilized platinum nanoparticles as effective oxidase mimics for colorimetric detection of acid phosphatase. *Nanoscale* **2017**, *9*, 10292–10300. [[CrossRef](#)]
16. He, W.; Liu, Y.; Yuan, J.; Yin, J.; Wu, X.; Hu, X.; Zhang, K.; Liu, J.; Chen, C.; Ji, Y. Au@Pt nanostructures as oxidase and peroxidase mimetics for use in immunoassays. *Biomaterials* **2011**, *32*, 1139–1147. [[CrossRef](#)] [[PubMed](#)]
17. Pal, J.; Pal, T. Enzyme mimicking inorganic hybrid Ni@MnO₂ for colorimetric detection of uric acid in serum samples. *RSC Adv.* **2016**, *6*, 83738–83747. [[CrossRef](#)]
18. Xia, M.; Chu, S.; Wang, S.; Dong, X.; Chen, C.; Jiang, Y.; Li, Z.; Lu, Y. Platinum nanoparticles confined in metal-organic frameworks as excellent peroxidase-like nanozymes for detection of uric acid. *Anal. Bioanal. Chem.* **2022**, *415*, 649–658. [[CrossRef](#)]
19. Wang, A.; Guan, C.; Shan, G.; Chen, Y.; Wang, C.; Liu, Y. A nanocomposite prepared from silver nanoparticles and carbon dots with peroxidase mimicking activity for colorimetric and SERS-based determination of uric acid. *Microchim. Acta* **2019**, *186*, 644. [[CrossRef](#)] [[PubMed](#)]
20. Ding, S.; Wang, W. Covalent organic frameworks (COFs): From design to applications. *Chem. Soc. Rev.* **2013**, *42*, 548–568. [[CrossRef](#)]
21. Pachfule, P.; Acharjya, A.; Roeser, J.; Sivasankaran, R.; Ye, M.; Bruckner, A.; Schmidt, J.; Thomas, A. Donor-acceptor covalent organic frameworks for visible light induced free radical polymerization. *Chem. Sci.* **2019**, *10*, 8316–8322. [[CrossRef](#)]
22. Li, G.; Tian, W.; Zhong, C.; Yang, Y.; Lin, Z. Construction of donor-acceptor heteroporous covalent organic frameworks as photoregulated oxidase-like nanozymes for sensing signal amplification. *ACS Appl. Mater. Interfaces* **2022**, *14*, 21750–21757. [[CrossRef](#)] [[PubMed](#)]
23. Xu, Y.; Wei, J.; Chen, X. Light-responsive sulfone-based covalent organic framework as metal-free nanoenzyme for visual colorimetric determination of uranium. *Chemosensors* **2022**, *10*, 248. [[CrossRef](#)]
24. Xu, L.; Chen, Y.; Yu, M.; Hou, M.; Gong, G.; Tan, H.; Li, N.; Xu, J. NIR light-induced rapid self-healing hydrogel toward multifunctional applications in sensing. *Nano Energy* **2023**, *107*, 108119. [[CrossRef](#)]
25. Luo, Y.; Yu, M.; Zhang, Y.; Wang, Y.; Long, L.; Tan, H.; Li, N.; Xu, L.; Xu, J. Highly sensitive strain sensor and self-powered triboelectric nanogenerator using a fully physical crosslinked double-network conductive hydrogel. *Nano Energy* **2023**, *104*, 107955. [[CrossRef](#)]
26. Xu, J.; Zhang, H.; Guo, Z.; Zhang, C.; Tan, H.; Gong, G.; Yu, M.; Xu, L. Fully physical crosslinked BSA-based conductive hydrogels with high strength and fast self-recovery for human motion and wireless electrocardiogram sensing. *Nano Energy* **2023**, *230*, 123195. [[CrossRef](#)]
27. He, Y.; Qi, F.; Niu, X.; Zhang, W.; Zhang, X.; Pan, J. Uricase-free on-demand colorimetric biosensing of uric acid enabled by integrated CoP nanosheet arrays as a monolithic peroxidase mimic. *Anal. Chim. Acta* **2018**, *1021*, 113–120. [[CrossRef](#)]
28. Ma, X.; Xu, W.; Liang, X.; Qiu, J. Low-temperature and gram-scale synthesis of chemically stable covalent organic frameworks in an aqueous medium. *New J. Chem.* **2022**, *46*, 4558–4561. [[CrossRef](#)]
29. Shinde, D.; Aiyappa, H.; Bhadra, M.; Biswal, B.; Wadge, P.; Kandambeth, S.; Garai, B.; Kundu, T.; Kurungot, S.; Banerjee, R. A mechanochemically synthesized covalent organic framework as a proton-conducting solid electrolyte. *J. Mater. Chem. A* **2016**, *4*, 2682–2690. [[CrossRef](#)]
30. Kaczmarek, A.; Liu, Y.; Kaczmarek, M.; Liu, H.; Artizzu, F.; Carlos, L.; Van Der Voort, P. Developing luminescent ratiometric thermometers based on a covalent organic framework (COF). *Angew. Chem. Int. Ed.* **2020**, *59*, 1932–1940. [[CrossRef](#)]
31. Wu, D.; Xu, Q.; Qian, J.; Li, X.; Sun, Y. Bimetallic covalent organic frameworks for constructing multifunctional Electrocatalyst. *Chem. Eur. J.* **2019**, *25*, 3105–3111. [[CrossRef](#)] [[PubMed](#)]
32. Chen, H.; Gu, Z.; Zhang, J. Chiral-induced ultrathin covalent organic frameworks nanosheets with tunable circularly polarized luminescence. *J. Am. Chem. Soc.* **2022**, *144*, 7245–7252. [[CrossRef](#)] [[PubMed](#)]
33. Wu, Z.; Huang, X.; Li, X.; Hai, G.; Li, B.; Wang, G. Covalent-organic frameworks with keto-enol tautomerism for efficient photocatalytic oxidative coupling of amines to imines under visible light. *Sci. China Chem.* **2021**, *64*, 2169–2179. [[CrossRef](#)]
34. Wang, X.; Tang, C.; Liu, J.; Zhang, H.; Wang, J. Ultra-small CuS nanoparticles as peroxidase mimetics for sensitive and colorimetric detection of uric acid in human serum. *Chin. J. Anal. Chem.* **2018**, *46*, E1825–E1831. [[CrossRef](#)]

35. Wu, Y.; Ma, Y.; Xu, G.; Wei, F.; Ma, Y.; Song, Q.; Wang, X.; Tang, T.; Song, Y.; Shi, M. Metal-organic framework coated Fe₃O₄ magnetic nanoparticles with peroxidase-like activity for colorimetric sensing of cholesterol. *Sens. Actuators B Chem.* **2017**, *249*, 195–202. [[CrossRef](#)]
36. Lu, Q.; Deng, J.; Hou, Y.; Wang, H.; Li, H.; Zhang, Y. One-step electrochemical synthesis of ultrathin graphitic carbon nitride nanosheets and their application to the detection of uric acid. *ChemComm* **2015**, *51*, 12251–12253. [[CrossRef](#)]
37. Tripathi, A.; Harris, K.; Elias, A. Peroxidase-like behavior of Ni thin films deposited by glancing angle deposition for enzyme-free uric acid sensing. *ACS Omega* **2020**, *5*, 9123–9130. [[CrossRef](#)]
38. Fang, A.; Wu, Q.; Lu, Q.; Chen, H.; Li, H.; Liu, M.; Zhang, Y.; Yao, S. Upconversion ratiometric fluorescence and colorimetric dual-readout assay for uric acid. *Biosens. Bioelectron.* **2016**, *86*, 664–670. [[CrossRef](#)]
39. Wang, X.; Zhu, G.; Cao, W.; Liu, Z.; Pan, C.; Hu, W.; Zhao, W.; Sun, J. A novel ratiometric fluorescent probe for the detection of uric acid in human blood based on H₂O₂-mediated fluorescence quenching of gold/silver nanoclusters. *Talanta* **2018**, *191*, 46–53. [[CrossRef](#)]
40. Yao, D.; Vlessidis, A.; Evmiridis, N. Microdialysis sampling and monitoring of uric acid in vivo by a chemiluminescence reaction and an enzyme on immobilized chitosan support membrane. *Anal. Chim. Acta* **2003**, *478*, 23–30. [[CrossRef](#)]
41. dos Santos, P.; Katic, V.; Toledo, K.; Bonacin, J. Photochemical one-pot synthesis of reduced graphene oxide/prussian blue nanocomposite for simultaneous electrochemical detection of ascorbic acid, dopamine, and uric acid. *Sens. Actuators B Chem.* **2018**, *255*, 2437–2447.
42. International Telecommunication Union. Studio Encoding Parameters of Digital Television for Standard 4:3 and Wide-Screen 16:9 Aspect Ratios. Available online: <https://www.itu.int/pub/R-REC/en> (accessed on 31 March 2023).
43. Yue, J.; Song, L.; Wang, Y.; Yang, P.; Ma, Y.; Tang, B. Fluorescence/colorimetry/smartphone triple-mode sensing of dopamine by a cof-based peroxidase-mimic platform. *Anal. Chem.* **2022**, *94*, 14419–14425. [[CrossRef](#)] [[PubMed](#)]

Disclaimer/Publisher's Note: The statements, opinions and data contained in all publications are solely those of the individual author(s) and contributor(s) and not of MDPI and/or the editor(s). MDPI and/or the editor(s) disclaim responsibility for any injury to people or property resulting from any ideas, methods, instructions or products referred to in the content.